THE JOURNAL OF PHYSICAL CHEMISTRY C

ARTICLE

pubs.acs.org/JPCC

High Temperature Water Gas Shift Reaction over Nanocrystalline Copper Codoped-Modified Ferrites

Gunugunuri K. Reddy,[†] Kapila Gunasekera,[‡] P. Boolchand,[*,‡] Junhang Dong,[†] and Panagiotis G. Smirniotis[*,†]

[†]Department of Chemical and Materials Engineering, and [‡]Department of Electrical and Computer Science Engineering, University of Cincinnati, Cincinnati, Ohio 45221, United States

ABSTRACT: Nanocrystalline metal (M)-modified ferrite catalysts co-doped with copper in atomic ratios Fe/M/Cu = 10/1/0.25 are synthesized and investigated for the high temperature water gas shift (WGS) reaction. The metal modifiers considered in the present work include M = Cr, Ce, Ni, Co, Mn, and Zn. The goal of the present work is to elucidate the role of Cu-codoping in the M-modified ferrites (Fe:M) for the WGS reaction. Interestingly, our shift activity results reveal that Cu act as a promoter for the modified ferrite catalysts, M = Cr, Ni, Co, Mn, and Zn, but it acts as an inhibitor for the case of cerium. XRD measurements indicate that there is a formation of solid solution of type $Fe_{0.875}M_{0.1}Cu_{0.025}$ (M = Cr, Ce, Ni, Co, Mn, and Zn) in the case of all copper doped-modified ferrites during the activation of the catalysts except for the case of cerium. The activated catalyst Fe/Ce/Cu shows magnetite and wustite phases in the XRD pattern. Cell parameter measurements show that Cu enters into the magnetite structure during the activation and leads to lattice expansion. Temperature-programmed reduction measurements inferred that Cu selectively promotes the reduction of hematite (Fe_2O_3) to magnetite (Fe_3O_4) in all modified ferrite catalysts. The addition of Cu to the Fe:Ce catalyst decreases significantly the reduction temperature of surface ceria, first, the transition temperature of hematite to magnetite, and, finally, the transition of magnetite to wustite. Mössbauer spectroscopic studies show changes both in the internal magnetic field and in the isomer shift parameters upon Cu-codoping, consistent with a lattice expansion of the magnetite phase. Our XRD and Mössbauer effect results suggest that Cu enters at M-modified octahedral sites in magnetite during activation of the catalysts and, in general, promotes the WGS activity.

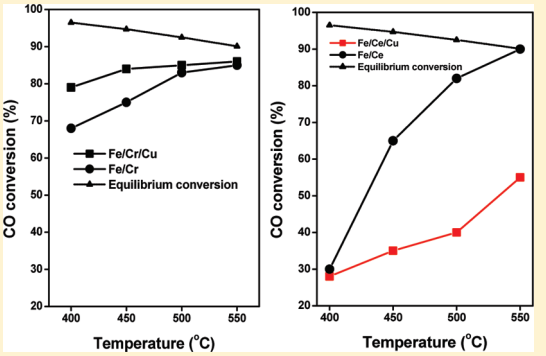

1. INTRODUCTION

Iron-containing spinels, also known as ferrospinels, are widely used catalysts for the water gas shift (WGS) reaction. The catalytic activity of spinels containing transition metal ions as dopants or modifiers is influenced by the acid−base and redox properties of these ions as well as by their site occupancy amongst the octahedral and tetrahedral sites in the spinel structure. It has been established that the octahedral sites are almost exclusively exposed at the surface of the spinel crystallites and that the catalytic activity is mainly due to octahedral cations.[1,2] In our earlier study, we modified iron oxide spinel (Fe:M) with selected transition metals (M = Cr, Mn, Co, Ni, Cu, Zn, and Ce) and catalytically examined them for the high temperature WGS reaction.[3] Among the various M-modified catalysts investigated, both Fe:Cr and Fe:Ce spinels in atomic ratio of 10:1 exhibited the highest activity. It is well-known that Cu is a promoter for both the low and the high temperature WGS reactions, although its promotional function is still debated.[4] One argument is that Cu provides active sites via formation of active Cu alloys. Cu doping into the iron oxide modifies the acid−base and redox properties of the spinel lattice. Rhodes and Hutchings[5] reported that Cu codoping into the Fe/Cr oxide decreases the reduction temperature of hematite to magnetite phase. The physical and chemical state of the Cu dopant on the surface plays an important role in the WGS reaction.[6] Other recent studies have also revealed that active Cu metal with partial ionic character present in the interface of nanoparticles and the support influences the activity of the catalyst.[7−10] Higher loading of CuO on oxide supports can lead to bigger particles and reduced activity.[11] Moreover, pyrophoricity also increases with Cu loading. Usually, impregnation methods are employed for metal loading on the surface of the supports. However, the coprecipitation method stabilizes the Cu in its ionic form. In this approach, a simultaneous precipitation of component hydroxides in the precursor may aid in the surface incorporation of Cu^{2+} ions.[12] Hence, all of the catalysts were prepared by coprecipitation method.

The present study mainly aimed at developing new series high temperature catalysts for the WGS reaction that can operate in extreme conditions, as posed in the membrane reactor regime. For this purpose, a series of Cu codoped-modified ferrites of type Fe:M:Cu with M = Cr, Ce, Ni, Co, Mn, and Zn with the chemical composition 10:1:0.25 atomic ratios were synthesized. High temperature WGS has been carried out over these modified ferrites in the temperature region of 400−550 °C and steam to

Received: January 11, 2011
Revised: March 10, 2011
Published: March 29, 2011

CO ratio of 3.5. A relatively high space velocity of 60 000 h^{-1} was maintained in the WGS reactor. Interestingly, by codoping with copper into the ferrospinels, we observed a quite different behavior in Fe/Cr in comparison to the Fe/Ce catalyst formulations. More specifically, Cu acts as a promoter for the Fe/Cr, while it acts as an inhibitor for the Fe/Ce catalyst. From our XRD and Mössbauer spectroscopic results, we concluded that codoping Cu in the Fe/Ce spinel leads to the formation of wustite (FeO) phase during the activation of the catalyst, thus resulting in a decreased catalytic activity. These findings stimulated us to comprehensively investigate the effect of Cu codoping on the structure and WGS activity of other transition metal doped ferrites, that is, Ni, Co, Mn, and Zn ferrites. From our observations, we can classify the modified ferrites into two categories, the first one where Cu has promotional effects (Cr-like-modified ferrites) and the other category where Cu has inhibition effects (Ce-like-modified ferrites).

2. EXPERIMENTAL SECTION

2.1. Catalyst Preparation. The ammonia-assisted coprecipitation route is used for high-yield preparations of various modified spinels Fe/M (M = Ce, Cr, Ni, Co, Mn, and Zn) and Cu codoped M- modified spinels Fe/M/Cu (M = Ce, Cr, Ni, Co, Mn, and Zn) for varying iron to metal ratios. In a typical preparation, calculated amounts of iron nitrate and metal dopant nitrate are dissolved separately in deionized water, and the aqueous solutions are mixed. Dilute aqueous ammonia was added gradually dropwise to the mixture solutions and vigorously stirred, until precipitation was complete (pH $\approx$ 8.5). The supernatant liquid was analyzed for nitrate ions by adding about 1 mL of concentrated sulfuric acid to 10 mL of the supernatant, while the formation of $[Fe(NO)]^{2+}$ can be detected by a brown ring.[13] In our experiments, in all cases the brown ring was not observed. The obtained precipitate gels were further aged overnight and filtered off. The obtained cakes were oven-dried at 80 °C for 12 h, and finally calcined at 500 °C for 3 h in an inert environment. The rate of heating as well as cooling was kept at 5 °C min^{-1}. The catalysts reported here could be prepared by the procedure above, permitting a direct comparison of their catalytic properties.[14]

2.2. Catalyst Characterization. *2.2.1. Surface Area and Pore Size Distribution Analysis.* The BET surface areas were obtained by N_2 adsorption on a Micromeritics ASAP 2010 Instrument. Prior to the analysis, samples were oven-dried at 120 °C for 12 h and flushed with argon for 2 h. The pore size distribution analyses were conducted by N_2 physisorption at liquid N_2 temperature using Micromeritics ASAP 2010 apparatus. All samples were degassed at 300 °C under vacuum before analysis.

2.2.2. X-ray Diffraction Measurements. Powder X-ray diffraction (XRD) patterns were recorded on a Phillips Xpert diffractometer using nickel-filtered Cu Kα (0.154056 nm) radiation source. The 0−80 °C were collected using 0.02° step size and a counting time of 1 s per point. Crystalline phases were identified by comparing the observed reflections with the reference ones from ICDD files. The average crystallite size of Fe_2O_3 was estimated with the help of the Debye−Scherrer equation, using the XRD data of all prominent lines.[15] Lattice parameters were established by employing standard indexation methods using the intensity of high 2θ peaks (300).[15−17]

2.2.3. TPR Measurements. The temperature-programmed reduction (TPR) with hydrogen of various catalyst samples was performed by means of an automated catalyst characterization system (Micromeritics, model AutoChem II 2920), which incorporates a thermal conductivity detector (TCD). The experiments were carried out at a heating rate of 5 °C/min. The reactive gas composition was H_2 (10 vol. %) in argon. The flow rate was fixed at 10 mL/min (STP). The TPR measurements were carried out following activation after cooling the sample in helium flow to 50 °C. The sample was then held at 50 °C under flowing helium to remove the remaining adsorbed oxygen until the TCD signal returned to the baseline. Subsequently, the TPR experiments were performed up to a temperature of 800 °C. The water formed during the reduction was removed by using an ice trapper. The gas stream coming from the reactor was passed through a trapper before the gas entered into the GC. A mixture of isopropanol and liquid nitrogen was used in the trapper to remove the formed water during the TPR experiment.

2.2.4. Mössbauer Spectroscopy. ^{57}Fe Mössbauer spectra were recorded in a transmission geometry using a constant acceleration spectrometer with liquid helium metal dewar.[18] Experiments were performed at room temperature. A 20 mCi of ^{57}Co (Rh) was used as an emitter, and the spectrometer was calibrated using an α-Fe foil, taking the isomer shift of Rh with respect to α-Fe at −0.15 mm s^{-1}. Line widths on the inner two lines of α-Fe were typically found to be 0.22 mm/s. An 80 mg quantity of the oxide catalyst as a fine powder was spread on a thin Teflon sheet using GE varnish as a binder and was used as an absorber. Typical runs lasted 48 h, and baseline counts per channel of two millions were collected. Mössbauer spectroscopy of activated catalysts was also measured. The catalyst was mixed with GE varnish in a nitrogen hood to prevent hydrolysis from ambient air. Line shapes were least-squares fitted to a superposition of the appropriate set of singlets and doublets to extract the hyperfine structure parameters hyperfine field (H), qudrapole splitting (Δ), and isomer shift (δ), and these data appear in Table 3.

2.3. Catalyst Activity. The WGS reaction was carried out in a vertical down flow fixed bed differential ceramic microreactor (i.d. 0.635 cm) at atmospheric pressure. In a typical experiment, ca. 0.1 g of powdered catalyst was placed between two plugs of quartz wool. The reactor was placed vertically inside a programmable tubular furnace (Lindberg), which was heated electrically. The catalyst pretreatment involves the partial reduction of hematite (Fe_2O_3) to magnetite (Fe_3O_4) using a process gas (mixture of H_2, CO, CO_2 (99.9% pure gases), and water vapor)[19−21] with a reductant to oxidant ratio of 1.4. Prior to the reaction, the catalyst was pretreated in flowing process gas at 400 °C for 4 h. It is important to avoid overreduction of the magnetite active phase to lower carbides, oxides, or metallic iron phases. Iron carbide phases are active catalysts for methanation and Fischer−Tropsch processes.[19] The rate of heating and cooling was always maintained at 5 °C min^{-1}. The gas flows were regulated through precalibrated mass flow controllers with digital read-out unit (MKS instruments). Water was injected into the system through a motorized syringe pump (Cole-Parmer type 74900) to generate steam. The entire system was kept at 200 °C by using heating tapes. Before pretreatment, the reactor setup was flushed with an inert gas, and the pretreatment gas mixture was initialized only after the catalytic system had attained temperature higher than 150 °C. The experiments were performed in the temperature region of 400−550 °C using a constant steam to CO ratio of 3.5. The gas hourly space velocity of 60 000 h^{-1} was maintained in all of the experiments. The product stream coming out from the reactor was passed through an ice cooled trap to condense water, after which the product gases were analyzed with an online TCD (Gow Mac series 550 thermal conductivity detector) having a porapak Q column for separation of the gases. This TCD

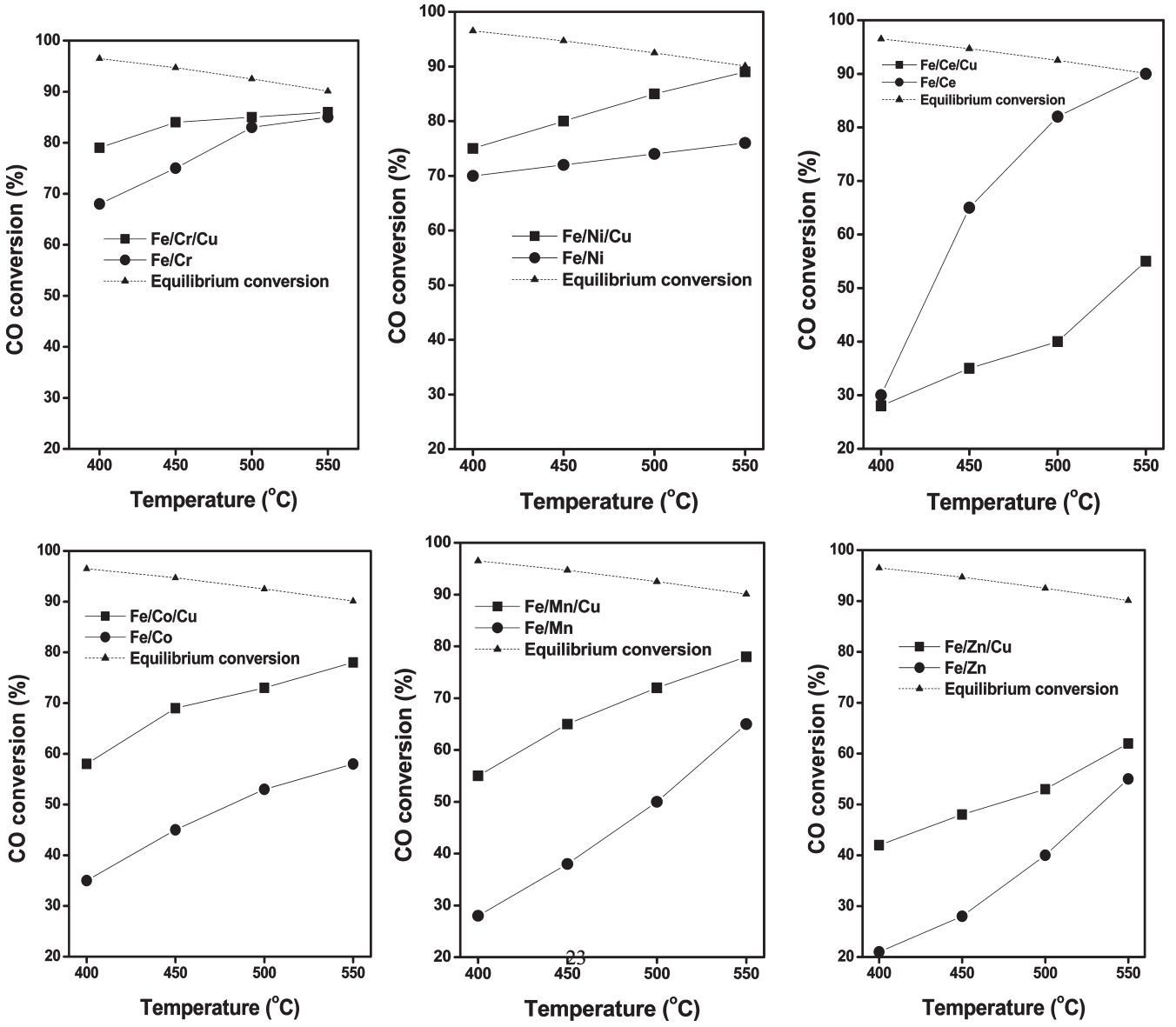

Figure 1. WGS activity results of various M-modified and copper codoped-modified ferrite catalysts (WHSV = 60 000 h^{-1}, steam to CO ratio 3.5).

was interfaced to a personal computer using a peak simple chromatography data system. The post analyses of results were done on the peak simple 2.31 software. The product-gas was injected through a six-port valve, and sampling was performed every 20 min interval. Reported values of conversions correspond to steady-state values at 0.5 h on stream.

3. RESULTS AND DISCUSSION

WGS Activity. High temperature WGS reaction has been carried out over M-modified and Cu codoped-modified ferrites in the temperature region of 400−550 °C and at total atmospheric pressure. In this study, WGS reaction was performed at a constant steam to CO ratio of 3.5. A relatively high space velocity of 60 000 h^{-1} was maintained in all of the experiments. On the whole, the WGS operating conditions were chosen to mimic conditions found in a membrane reactor. Before the reaction, all of the ferrite catalysts are activated in the presence of process gas at 400 °C for 4 h. During the activation, all of the catalysts are transformed from the hematitic phase to the magnetite phase. It is important to avoid over-reduction of the magnetite active material during the activation process to lower oxides, wustite, or metallic iron species. The iron carbide species especially are active catalysts for the Fischer−Tropsch process, thus leading to methanation in the WGS reaction.[22] The ratio of oxidant to reductant (also called "reduction factor, R") in the process gas mixture has to be just optimal, to facilitate the reduction of hematitic to magnetite phase, and should not catalyze further reduction. In the present study, R = 1.4 was utilized, where $R = [(CO) + (H_2)]/[(CO_2) + (H_2O)]$. WGS activity profiles of various M-modified and copper codoped-modified ferrites are presented in Figure 1. In general, with increasing temperature the WGS activity was found to increase. No pressure drop across the catalyst bed was observed during the experiments. Methane formation was observed in the case of both Fe/Mn and Fe/Mn/Cu catalysts due to Fischer−Tropsch (FT) reaction. Interestingly, shift activity results reveal that copper acts as a promoter

dx.doi.org/10.1021/jp2003084 |J. Phys. Chem. C 2011, 115, 7586–7595

for the modified ferrite catalysts except Fe/Ce catalyst. It acts as an inhibitor for the Fe/Ce catalyst. These results show that all of the copper codoped ferrites behave like Fe/Cr/Cu except for Fe/Ce/Cu, which behaves differently for high temperature WGS reaction. We explained this interesting behavior of copper based on the various characterization techniques like Mössbauer, TPR, and XRD. Among the various catalysts, Fe/Ce, Fe/Cr/Cu, and Fe/Ni/Cu reached equilibrium conversions at the highest reaction temperature (550 °C) investigated. When the reaction temperature increased from 400 to 500 °C, the activity of Fe/Ce increased from 30% to 82%. The higher activity of Fe/Ce at higher reaction temperature is because both iron and ceria undergo a facile charge transfer reaction between $Fe^{III} \leftrightarrow Fe^{II}$ and $Ce^{IV} \leftrightarrow Ce^{III}$ redox couples, respectively; the synergism between the two couples could be responsible for the improved WGS activity.[1] Additionally, at higher temperatures, the rapid transformation of oxygen exchange between Ce^{3+}/Ce^{4+} redox couple, as well as the improvement in the oxygen storage capacity of ceria,[23] will help the iron to keep its shift activity high.

Structural and Surface Properties. The X-ray diffraction patterns have been collected on the surfaces of the disks with a Rigaku diffractometer using Cu Kα radiation. Figure 2 shows the representative 2θ scans of XRD for the Cu^{2+} codoped-modified ferrite catalysts. The corresponding crystallite sizes of the Cu codoped samples are presented in Table 1. The entire copper codoped samples exhibit less intense peaks as compared to the M-modified ferrites (not shown). The existence of an Fe_2O_3 type phase (PDF-ICDD 33-0664) was identified by comparison with standard reference data from the PDF database. The powder diffraction analyses indicate the presence of the pure hematite crystalline phase with the reflections (012), (104), (110), (113), (024), (116), (214), and (300).[24] The observation of hematite phase in all of the catalysts is of significant importance in the present investigation because during the catalyst activation the hematite phase is converted to the magnetite phase (Fe_3O_4), which is the active phase for the high temperature WGS reaction. Additionally, the XRD patterns of the copper codoped modified ferrite samples do not show any extra crystalline phases due to either copper or compounds between copper and iron. As per the literature reports, both Fe and Cu can form $CuFe_2O_4$ spinels very easily when mixed together. In the present study, we did not observe any formation of such spinels for our Cu codoped-modified ferrites. This is due to the lower doping amount of copper (2.5%) used in this study.

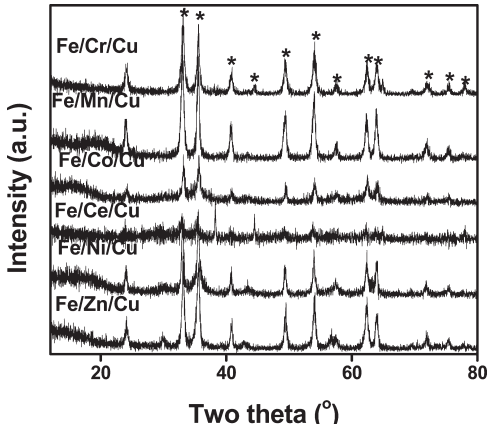

Figure 2. X-ray powder diffraction patterns of copper codoped-modified ferrite fresh catalysts (*, Fe_2O_3).

The X-ray powder diffraction patterns of activated M-modified and Cu codoped-modified ferrite catalysts are presented in Figure 3. All of the activated catalysts except Fe/Ce/Cu catalyst exhibit intense diffraction lines at 2θ values 30°, 35°, 43°, 57°, 62°, and 73°. These peaks could be indexed as that of cubic system with face-centered lattice. For M-modified ferrites and Cu codoped-modified ferrite samples, the strongest Bragg peak occurs at 2θ = 35.9° corresponding to the (311) reflections. The above indexed peak is consistent with the Joint committee for powder diffraction (JCPD) data.[15] On the other hand, the Fe/Ce/Cu catalyst exhibits a few additional diffraction lines at 2θ = 36°, 41°, and 60°. These peaks primarily belong to the wustite (FeO) phase.[15] These results indicate that simultaneous precipitation of Fe along with Ce and Cu leads to the formation of FeO during the activation. We know that FeO is an inactive phase for the WGS reaction. The formation of FeO during the activation of Fe/Ce/Cu is responsible for the lower WGS activity as compared to the Fe/Ce catalyst. The TPR and Mössbauer spectroscopy results presented in latter sections also support this observation. The formation of wustite phase was not observed in the Fe/Ce catalysts. The formation of wustite was also not observed in other copper codoped-modified ferrites. These results show that all of the copper-modified ferrites behave like Fe/Cr/Cu, while only Fe/Ce/Cu behaves differently for high temperature WGS reaction. There was no evidence for the formation of Fe (metallic) or Fe_2C phases due to over-reductions in any of the M-modified or Cu codoped-modified ferrites. A shift in the peak positions toward lower angle side was observed in copper codoped ferrites as compared to the M-modified ferrites. This is due to the incorporation of the Cu^{2+} ions into the cubic magnetite lattice during the activation. These results indicate that there is a formation of a solid solution of type $Fe_{0.875}M_{0.1}Cu_{0.025}$ with M = Cr, Ce, Ni, Co, Mn, and Zn in the case of copper codoped-modified ferrites during the activation of the catalysts.

Table 1. BET Surface Area, Crystallite Size, and Pore Diameter Values of Various Copper Codoped-Modified Ferrite Fresh Catalysts[a]

sample	BET surface area (m^2/g)	crystallite size (nm)	pore diameter (nm)	composition of the catalysts by EDAX
Fe/Cr/Cu	98	11	63	9.8:1.05:0.26
Fe/Ce/Cu	126	nd	82	9.75:1.0:0.23
Fe/Ni/Cu	98	9.7	41	9.95:0.99:0.21
Fe/Co/Cu	80	5.8	88	9.9:0.95:0.25
Fe/Mn/Cu	175	17.9	110	9.8:1:0.24
Fe/Zn/Cu	53	22	113	10:1.1:0.24

[a] nd: Not determined.

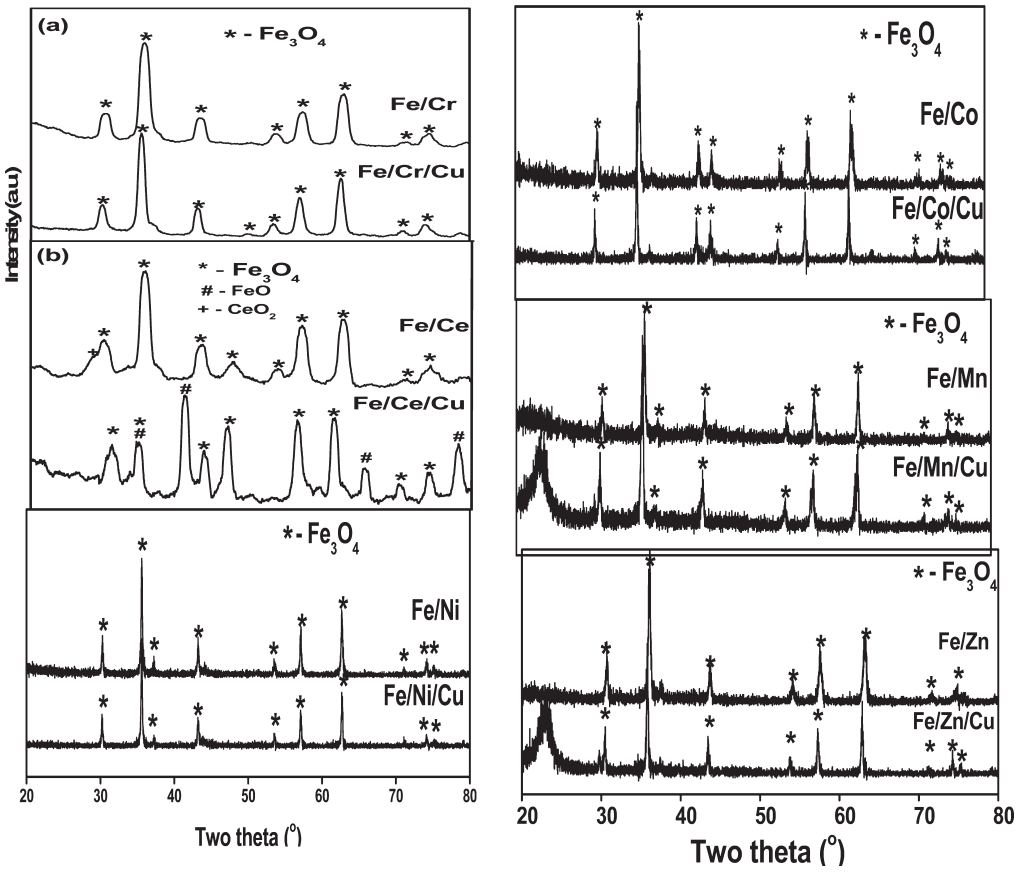

Figure 3. X-ray powder diffraction patterns of M-modified and copper codoped-modified ferrite activated catalysts (*, Fe_3O_4; +, CeO_2; #, FeO).

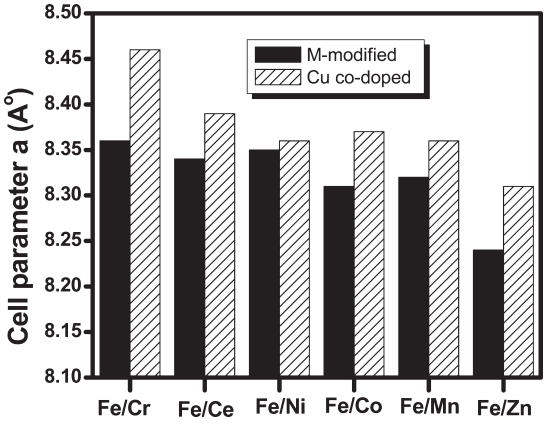

Figure 4. Cell parameter measurements plot of various M-modified and copper codoped-modified ferrite activated catalysts.

The BET surface area, pore size, and crystallite sizes of hematite of all of the Cu codoped-modified ferrite values are presented in Table 1. As one can observe, all of the copper codoped-modified ferrites exhibit higher surface area and lower crystallite sizes as compared to the M-modified ferrites. Hence, both XRD and crystallite size measurements suggest that all of the Cu codoped-modified ferrites exhibit nanocrystalline nature. The efficacy of the dopant ion in modifying the resultant surface area could be directly related to variations in the rate of crystal growth. The nature and amount of the foreign cations present in the system govern this variation. The increase in the surface area is primarily due to the formation of solid solution due to the incorporation of Cu^{2+} into the hematitic lattice. A broad particle size distribution in the range of 7.0−25 nm was observed for all of the investigated samples. Here, also all of the copper codoped M-modified ferrite catalysts exhibit smaller pore diameter as compared to M-modified ferrite catalysts. Using the interplanar spacing values, calculation of the cell parameters was carried out for the activated catalysts (Figure 4). This revealed that the Cu ions enter the hematite lattice under the activation conditions employed in this work. X-ray diffraction patterns reveal that activated catalysts exhibit peaks due to the magnetite phase which is a cubic lattice. Hence, the lattice constant values are measured from the (311) plane.[25] By comparing the values of the copper codoped-modified ferrite samples with that of the M-modified ferrite samples, prepared by an identical method, it is observed that the lattice expansion is taking place in the case of copper codoped samples. This is due to the fact that copper has larger ionic radii as compared to the both Fe^{3+} and Fe^{2+}. Hence, when copper is incorporated into the magnetite lattice, obviously it leads to the lattice expansion. Magnetite is a spinel and possesses both tetrahedral and octahedral iron sites.[26] With trivalent iron, there are five "d" electrons in the "3d" orbitals. In the high spin state, each of these would be unpaired and occupy all of the t_{2g} and e_g orbitals in an octahedrally coordinated environment or all of the t_2 and e sites in a tetrahedrally coordinated environment. Because there is no degeneracy, the CFSE for each of these coordinations is zero. Thus, there is no preference for either coordination. The alteration in the lattice parameter upon M^{n+} (substituent cation) substitution suggests the incorporation of M^{n+} into the spinel structure. The actual composition of the Cu codoped-modified ferrite

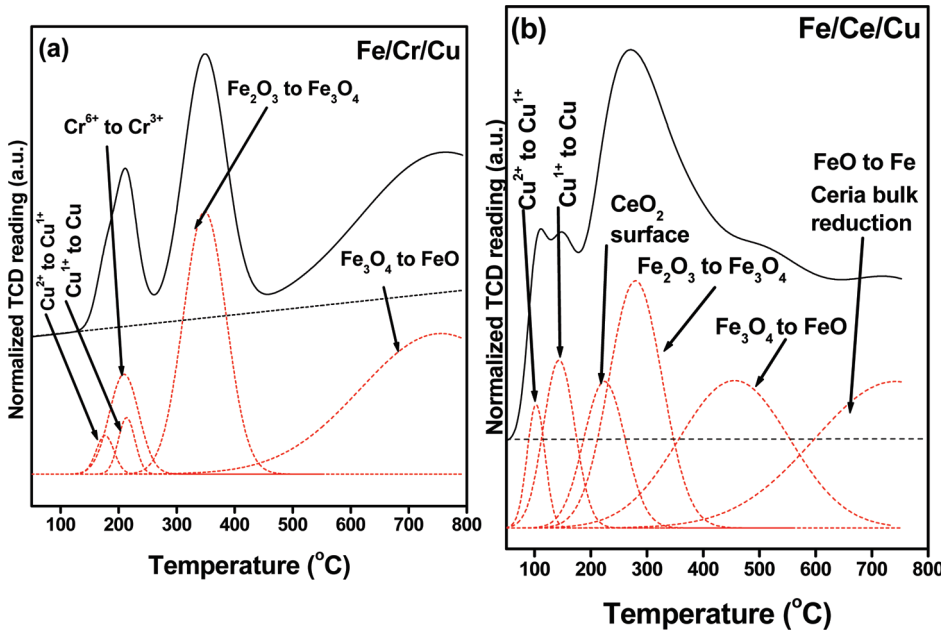

Figure 5. TPR profiles of Fe/Cr/Cu and Fe/Ce/Cu catalysts.

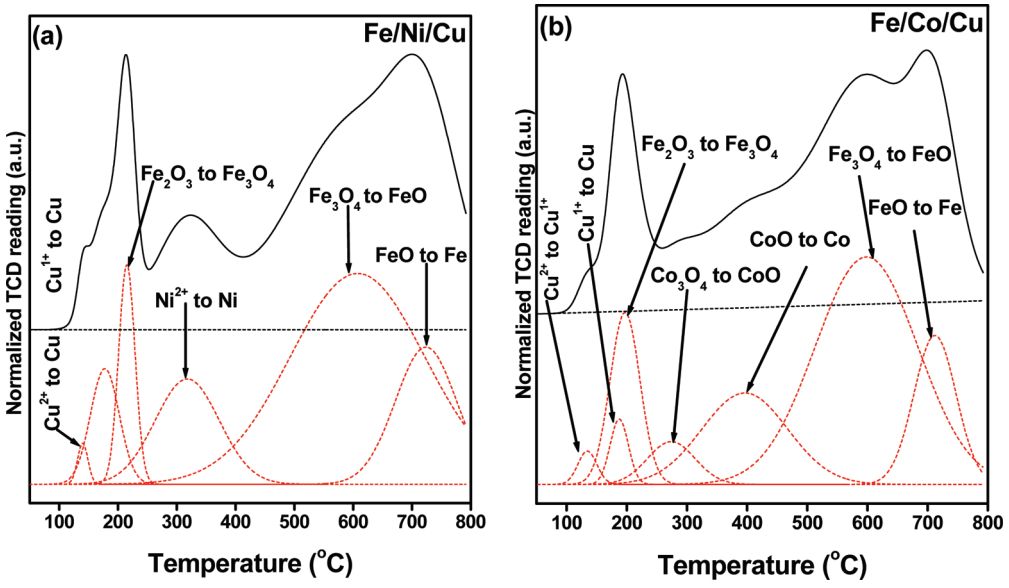

Figure 6. TPR profiles of Fe/Ni/Cu and Fe/Co/Cu catalysts.

catalysts was determined by EDAX technique, and the values are presented in Table 1. The values presented in Table 1 well agree with the experimental values.

TPR Measurements. Temperature programmed reduction experiments have been carried out over both M-modified and copper codoped-modified ferrites to understand the specific role of copper on the reducibility of iron oxide and T_{max} of phase transitions. The TPR profiles of the various Cu codoped iron oxide-based catalysts are presented in Figures 5, 6, and 7. The corresponding T_{max} values for each reduction step of iron oxide of both M-modified and copper codoped-modified ferrites are shown in Table 2. In the reported TPR of pure hematite (Fe_2O_3), the first reduction peak appears at 302 °C, corresponding to the transition of Fe_2O_3 to Fe_3O_4. The second peak at 354 °C was attributed to the transformation of Fe_3O_4 to FeO. The third and final peak at 475 °C corresponds to the transition of FeO to Fe.[27] In another report, the TPR curves of hematite showed a peak at 510 °C, attributed to magnetite formation, and another around 770 °C, attributed to the formation of metallic iron.[28] The position of the temperature maxima may vary from sample to sample depending on the particle size and other parameters such as temperature ramp rate. The addition of a substituent/dopant ion significantly modifies the reduction profile, as compared to that of the pristine Fe_2O_3 sample.[29]

From Figures 5−7 and Table 2, it is obvious that the effect of copper on the reduction profile of iron oxide depends on the other metal being presented in the ferrites, that is, Cr, Mn, Co, Ni, Cu, Zn, and Ce. In the present study, the TPR peaks were

dx.doi.org/10.1021/jp2003084 |J. Phys. Chem. C 2011, 115, 7586–7595

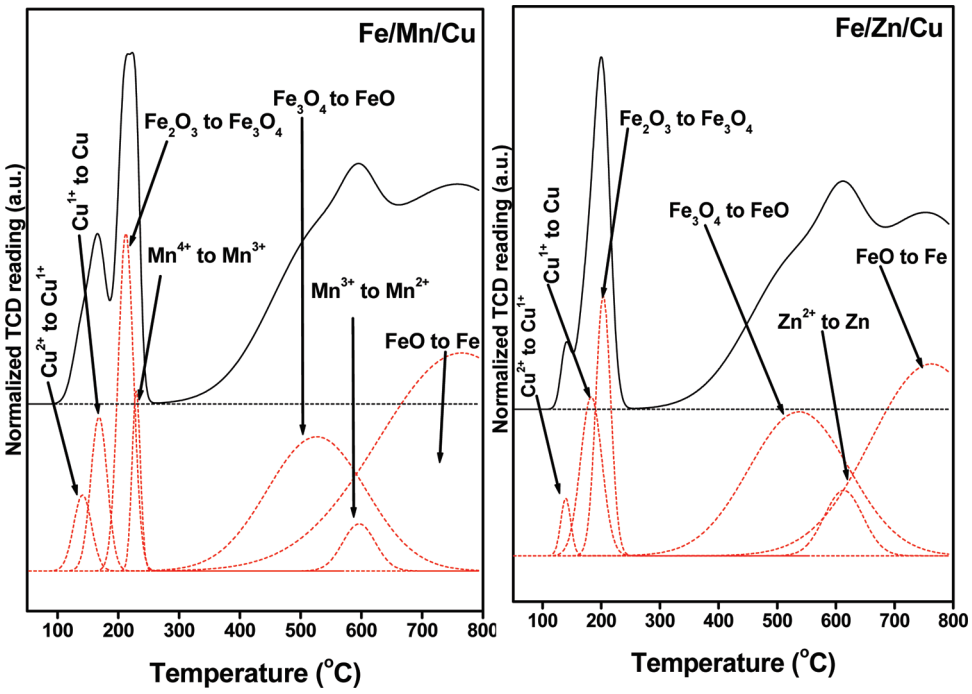

Figure 7. TPR profiles of Fe/Mn/Cu and Fe/Zn/Cu catalysts.

assigned on the basis of our previous results as well as literature reports. In our previous publication, we already reported the TPR profiles of M-modified ferrites and pristine oxides. Hence, in the present study, the TPR peaks were assigned on the basis of our previous results as well as literature reports. In the case of Fe/Cr/Cu catalyst, the first peak at 170 °C, which corresponds to the reduction of $Cu^{2+} \rightarrow Cu^{+}$ and further reduction to Cu^{0}, occurs at 220 °C. The second reduction peak was observed at 225 °C, which corresponds to the reduction of $Cr^{6+} \rightarrow Cr^{3+}$.[30] Further reduction of Cr^{3+} to metallic chromium was not observed. The addition of copper to the Fe/Cr-modified ferrite did not improve the reducibility of the $Cr^{6+} \rightarrow Cr^{3+}$ redox couple. Reduction of hematite (Fe_2O_3) to magnetite (Fe_3O_4) was observed at 350 °C. In the case of Fe/Cr, this reduction peak was observed at 400 °C. Hence, the addition of copper to the Fe/Cr-modified ferrite promotes the reduction of the hematite to magnetite transformation. Further reduction from Fe_3O_4 to FeO seems to start at about 500 °C. Copper did not promote the reduction of Fe_3O_4 to FeO transformation, as it occurs at the same temperature as Fe/Cr. Figure 5b represents the TPR profile of Fe/Ce/Cu catalyst, and the profile exhibits total six peaks. The first reduction peak occurs at 148 °C, corresponding to the reductive transition of Cu^{2+} to Cu^{1+}. Further reduction of Cu^{1+} to Cu^{0} occurs at 170 °C. The ceria surface reduction starts at 160 °C and reached a maximum at 220 °C. Further reduction starts at 160 °C due to the transformation of Fe_2O_3 to Fe_3O_4. In pure ceria, this reduction is observed at 485 °C, and in Fe/Ce it occurred at 308 °C.[31] A fifth reduction peak starts at 200 °C, which is due to the reduction of Fe_3O_4 to FeO. Interestingly, the addition of copper to the Fe/Ce promotes all three transformations, $Fe_2O_3 \rightarrow Fe_3O_4$, $Fe_3O_4 \rightarrow$ FeO, and surface ceria reduction to much lower temperatures as compared to the Fe/Ce sample. These results are corroborating with XRD measurements. XRD results also show that the formation of FeO during the activation of Fe/Ce/Cu at 400 °C does occur. Further reduction of bulk ceria and FeO to Fe occurs at higher temperature (500 °C).

Table 2. T_{max} (°C) Values of Various Phase Transformations of the M-Modified and Copper Codoped-Modified Ferrite Catalysts

sample	$Fe_2O_3 \rightarrow Fe_3O_4$	$Fe_3O_4 \rightarrow$ FeO
Fe/Cr/Cu	350	>700
Fe/Cr	429	>700
Fe/Ce/Cu	286	300
Fe/Ce	310	577
Fe/Ni/Cu	216	608
Fe/Ni	327	597
Fe/Co/Cu	196	598
Fe/Co	330	680
Fe/Mn/Cu	213	734
Fe/Mn	300	613
Fe/Zn/Cu	204	713
Fe/Zn	333	700

The TPR profile of Fe/Ni/Cu exhibits total six peaks. The reduction peaks due to $Cu^{2+} \rightarrow Cu^{+} \rightarrow Cu^{0}$ occur at 138 and 178 °C. Here also, doping with copper promotes the reduction of hematite to magnetite transformation, which occurred at 216 °C, while for the parent Fe/Ni catalyst it occurs at 327 °C.[31] Further reduction of magnetite to wustite is observed at 608 °C in Fe/Ni/Cu, while in the Fe/Ni it was observed at 597 °C. These results confirm that the addition of copper to the Fe/Ni did not promote the reduction of magnetite to wustite. As in the case of Fe/Cr catalysts, in this case also the addition of copper did not promote the reduction of NiO to metallic Ni, and it occurs at 313 °C.[31] The reduction of FeO to metallic iron started at higher temperatures (>700 °C). Fe/Ce/Co exhibits a total of seven peaks in the TPR profile. The first two peaks are due to the reduction of CuO and are observed at 158 and 210 °C. The reduction due to hematite to

dx.doi.org/10.1021/jp2003084 |J. Phys. Chem. C 2011, 115, 7586–7595

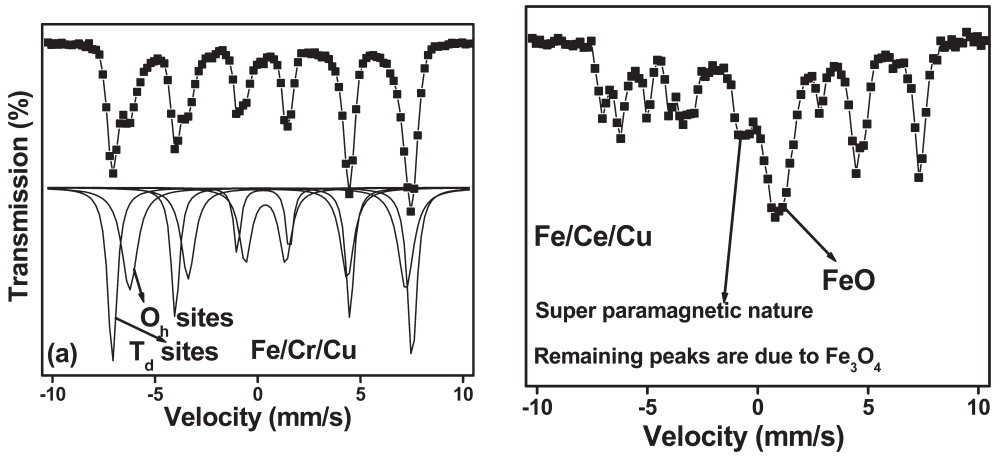

Figure 8. Room temperature Mossbauer spectroscopy data of activated Fe/Cr/Cu and Fe/Ce/Cu catalysts.

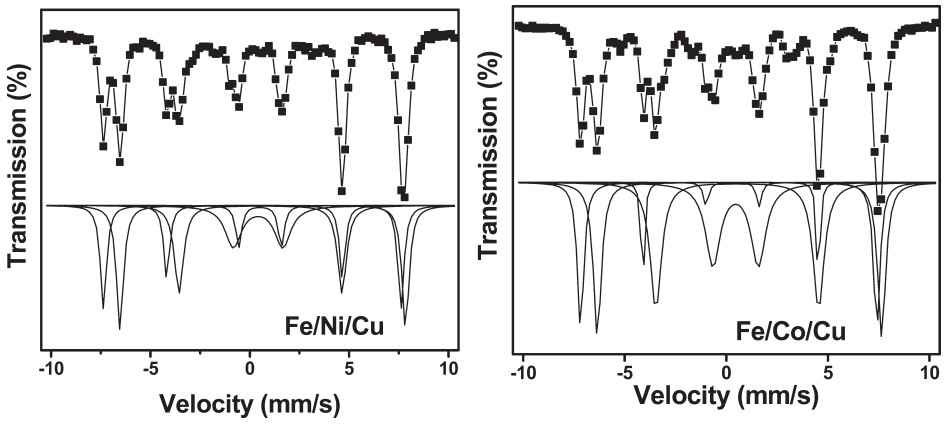

Figure 9. Room temperature Mossbauer spectroscopy data of activated Fe/Ni/Cu and Fe/Co/Cu catalysts.

magnetite was observed at a lower temperature of 196 °C as compared to the case of Fe/Co (330 °C) due to the promotional effect of copper. The reduction of Co_3O_4 to CoO and CoO metallic Co was then observed.[31] The reduction of magnetite to wustite was observed at higher temperature. The TPR profiles of Fe/Mn/Cu and Fe/Zn/Cu are very similar to that of Fe/Cr/Cu. The Fe/Mn/Cu exhibits a total of seven peaks in the TPR profile, and Fe/Zn/Cu exhibits a total of six peaks. In both profiles, the first two peaks are due to the $Cu^{2+} \rightarrow Cu^{1+} \rightarrow Cu^{o}$ transformations, respectively. In the Fe/Mn/Cu sample, the reduction of $Fe_2O_3 \rightarrow Fe_3O_4$ was observed at 213 °C, and in Fe/Zn/Cu it was observed at 204 °C, which are at much lower temperature as compared to the Fe/Mn (300 °C) and Fe/Zn (333 °C), respectively, which is due to the promotional effect of copper. In these cases, also copper did not promote either the reduction of magnetite to wustite or the reduction of other transition metal oxide, that is, MnO_2 and ZnO. On the whole, TPR measurements reveal that in all modified ferrites except Fe/Ce/Cu, copper promotes the reduction of hematite (Fe_2O_3) to magnetite (Fe_3O_4). Yet it does not promote either reduction of magnetite to wustite or reduction of other metal oxide present in the ferrite. On the other hand, in Fe/Ce/Cu catalyst, copper promotes the reduction of all three transformations, that is, hematite to magnetite, magnetite to wustite, and surface ceria reduction. This leads to the formation of wustite phase during the activation and causes the decrease of the WGS activity.

Mössbauer Spectroscopy Measurements. Mössbauer spectroscopy is a useful probe not only to investigate the magnetic phases but also to identify the Fe distribution at tetrahedral (A) and octahedral (B) sites.[32] Magnetite possesses an inverse spinel structure with oxygen ions forming a FCC close packed structure. The magnetic properties of magnetite have been broadly explained on the assumption that spins at octahedral and tetrahedral sites form two antiferromagnetically coupled sublattices.[33] At room temperature, magnetite gives two six-line patterns in a Mössbauer spectrum: one pattern is due to the Fe^{3+} ions at tetrahedral sites, while the other pattern comes from the presence of Fe^{2+} and Fe^{3+} ions at the octahedral sites.

To investigate structural changes of magnetite after activation, Mössbauer spectroscopy measurements were performed on M-modified and copper codoped-modified ferrites. X-ray diffraction results show that all of the M-modified and Cu codoped ferrites transformed from hematite to magnetite after the activation. The spectra are presented in Figures 8, 9, and 10. The hyperfine structures, such as isomer shift (δ), quadrapole splitting (Δ), and magnetic field (H), are summarized in Table 3. All of the M-modified and Cu codoped ferrites show similar Mössbauer spectra except for the cases of Fe/Ce and Fe/Ce/Cu. The typical spectra consist of two well-developed six-line magnetic hyperfine structure typical of bulk materials with no trace of superparamagnetic behavior (Figures 8−10). The high field component is due to Fe^{3+} ions at

dx.doi.org/10.1021/jp2003084 |J. Phys. Chem. C 2011, 115, 7586–7595

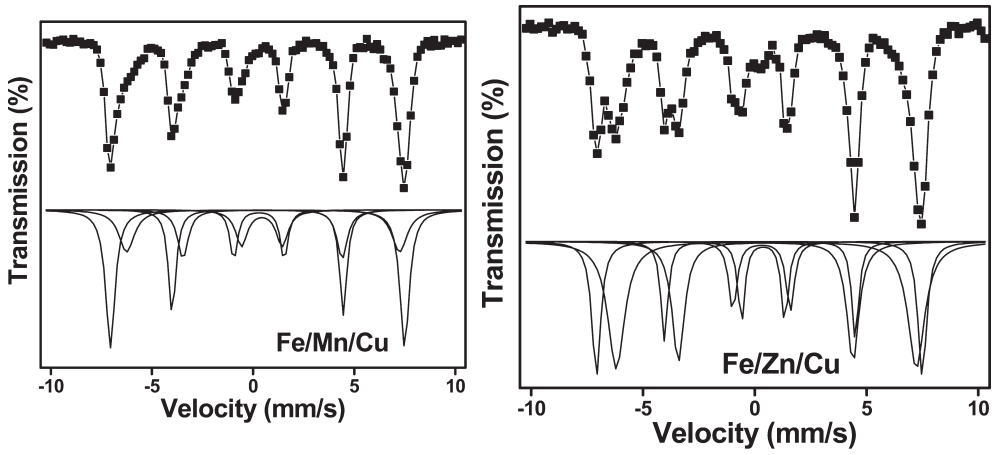

Figure 10. Room temperature Mossbauer spectroscopy data on activated Fe/Mn/Cu and Fe/Zn/Cu catalysts.

Table 3. Isomer Shift (δ), Magnetic Field (H), Quadrapole Splitting (Δ), and Concentration Ratio of Octahedral to Tetrahedral Sites in Various M-Modified and Copper Codoped-Modified Ferrite Catalysts[a]

	tetrahedral sites			octahedral sites			
sample	δ	Δ	H	δ	Δ	H	O_h/T_d occupancy
Fe/Cr/Cu	0.32	0	485	0.53	0.0	447	1.1
Fe/Cr	0.32	−0.02	513	0.47	0	475	2.54
Fe/Ce/Cu	nd	nd	nd	Nd	nd	nd	nd
Fe/Ce	0.33	−0.01	509	0.47	0	471	2.44
Fe/Ni/Cu	0.31	−0.062	480	0.53	0.065	460	1.3
Fe/Ni	0.31	−0.058	498	0.50	0.056	478	1.8
Fe/Co/Cu	0.3	−0.05	485	0.58	0.057	465	1.4
Fe/Co	0.32	−0.058	493	0.52	0.091	472	2.6
Fe/Mn/Cu	0.33	−0.003	484	0.49	−0.01	449	1.5
Fe/Mn	0.33	−0.012	487	0.47	−0.03	454	1.9
Fe/Zn/Cu	0.33	−0.01	485	0.48	0.015	446	1.6
Fe/Zn	0.33	0.01	489	0.47	0.011	440	1.9

[a] Isomer shifts are quoted relative to α-Fe at room temperature. The error in δ is ±0.02 mm/s, in Δ is ±0.02 mm/s, and in H is ±5 kOe.

tetrahedral sites, while the low field one arises from Fe^{2+} and Fe^{3+} ions present at octahedral sites.[34] The δ and H values presented in Table 3 are in good agreement with previous reports.[35−37] There is not much change in the δ and H values for Fe at tetrahedral sites after Cu codoping. On the other hand, δ and H values for octahedral sites in the Cu codoped-modified ferrite catalysts are noticeably higher than those for M-modified ferrite catalysts. Our XRD and Mössbauer effect results suggest that Cu enters at M-modified octahedral sites in magnetite during activation of the catalysts. The concentration ratio of O_h to T_d sites in copper codoped and M-modified ferrite catalysts is presented in Table 2. Generally, this ratio is close to 2 in pure activated Fe_2O_3 catalyst. All of the Cu codoped ferrite catalysts exhibit O_h/T_d ratios less than those in M-modified ferrite catalysts. These results show that Cu enters at octahedral sites of magnetite during activation of the catalysts and alters the local structure. The Mössbauer line shape of both Fe/Ce and Fe/Ce/Cu ferrite differs from other modified ferrites; in Fe/Ce catalyst, in addition to the two six-lines patterns, a singlet is observed at the center of the spectrum, that is, near zero velocity. This singlet is due to the super paramagnetic behavior of the catalysts, resulting from a collapse of H-field in the nanoparticles. Mössbauer spectra of Fe/Ce/Cu catalyst exhibit features from four total components, making it more challenging to obtain a line shape deconvolution. In addition to the peaks from the O_h sites, T_d sites, and super paramagnetic sites, one more peak at a velocity of 1.5 mm/s is observed. This peak is due to the formation of wustite (FeO) phase.[32]

Structure−Catalytic Activity Relationship. Copper codoped-modified ferrites of type Fe/M/Cu (M = Cr, Ce, Ni, Co, Mn, and Zn) with the chemical composition 10:1:0.25 were prepared by the deposition− precipitation method using nitrates as precursors. Our experiments show that the overall WGS activity depends on various parameters such as activation conditions, the nature of the M-modifier, and reaction conditions. Co-doping with Cu promotes the WGS activity of all of the modified ferrites except for Fe/Ce/Cu. On the other hand, Cu acts as an inhibitor for the Fe/Ce catalyst. Among the various catalysts investigated, Fe/Ce, Fe/Cr/Cu, and Fe/Ni/Cu catalysts exhibited equilibrium conversion at a reaction temperature of 550 °C. Addition of copper increases the BET surface area of the M-modified ferrites. XRD measurements reveal the formation of hematite phase in the fresh catalysts and magnetite phase in the activated catalysts except for Fe/Ce/Cu catalyst. Fe/Ce/Cu catalyst exhibited both magnetite and wustite phases in the activated catalyst. Cell parameter estimations suggest that copper enters into the magnetite lattice during the activation of the catalysts. TPR measurements reveal that the addition of copper to the modified ferrites with the exception of Fe/Ce/Cu shifts the temperature maxima of hematite to magnetite to lower temperatures and promotes the WGS activity. However, Cu does not promote the reduction of magnetite to wustite or reduction of other metal oxides present in the ferrite. On the other hand, the addition of Cu to the Fe/Ce catalyst brought down the reduction temperatures of hematite to magnetite, magnetite to wustite, and surface ceria reduction transformations. This leads to the formation of wustite phase during the activation of the Fe/Ce/Cu catalyst. Mössbauer spectroscopy measurements show that copper enters into the O_h sites of the magnetite cubic lattice during the activation and makes structural rearrangements in the lattice. On the whole, with the exception of cerium, all of the copper doped-modified ferrites behave like Cu doped Fe/Cr catalyst in which Cu acts as a promoter for WGS activity. In contrast, Cu acts as an inhibitor for the Fe/Ce catalyst.

4. CONCLUSIONS

High surface area nanocrystalline metal (M)-modified ferrites codoped with Cu were synthesized by precipitation of corresponding nitrates. Samples with M = Cr, Ce, Ni, Co, Mn, and Zn, and relative concentrations (atomic %) Fe:M:Cu = 10:1:0.25, were examined in the present work. Our goal here is to elucidate the role of Cu codoping on the catalytic performance of the M-modified ferrites in WGS reaction. Activation in a controlled atmosphere transformed the catalysts into magnetite spinels. The fresh and activated catalysts were characterized by XRD, BET, TPR, and Mössbauer spectroscopy. Cu codoping increases BET surface area of all M-modified ferrites. Furthermore, Cu codoping also lowers the hematite to magnetite conversion temperature and promotes WGS activity in all cases. Cu codoping neither promotes reduction of parent metal oxides, nor the reduction of magnetite to wustite for all metal dopants, except for the case of cerium. In the latter case, Cu codoping actually promotes the reduction of magnetite to wustite, and also of surface ceria that decrease the catalytic activity. During the activation, an increase of cell length upon Cu codoping is observed and suggests that the Cu guest enters the magnetite structure substititutionally. Indeed, Mössbauer spectroscopy confirms that the codoped Cu enters octahedral sites for all M-modified ferrites except for the case of cerium. For this case (cerium doped), activation of the catalyst leads to the formation of magnetite and wustite. Because of the presence of wustite, the performance of the Fe/Ce/Cu catalyst is lower than that of Fe/Ce. Among the various catalysts investigated here, Fe/Ce, Fe/Cr/Cu, and Fe/Ni/Cu exhibited equilibrium conversions at the highest reaction temperatures.

AUTHOR INFORMATION

Corresponding Author

*Tel.: (513) 556-1474. Fax: (513) 556-3473. E-mail: panagiotis.smirniotis@uc.edu (P.G.S.), boolchp@ucmail.uc.edu (P.B.).

ACKNOWLEDGMENT

Financial support was provided by the U.S. Department of Energy (grant DE-PS36-03GO93007). The financial support received from Ohio Air Quality Development Authority (AY08-09-C21) is also appreciated.

REFERENCES

(1) Boreskov, G. K. *Kinet. Catal.* **1970**, *11*, 374.
(2) Topsoe, H.; Boudart, M. *J. Catal.* **1973**, *31*, 346.
(3) Khan, A.; Chen, P.; Boolchand, P.; Smirniotis, P. *J. Catal.* **2008**, *253*, 91.
(4) Ratnasamy, C.; Wagner, J. P. *Catal. Rev.-Sci. Eng.* **2009**, *51*, 325.
(5) Rhodes, C.; Hutchings, G. J. *Phys. Chem. Chem. Phys.* **2003**, *5*, 2719.
(6) Idakiev, V.; Mihajlo, A. D.; Kanev, B.; Andreev, A. *React. Kinet. Catal. Lett.* **1987**, *33*, 119.
(7) Andreev, A.; Idakiev, V.; Mihajlova, D.; Shopov, D. *Appl. Catal.* **1986**, *22*, 385.
(8) Chen, C. S.; Lin, J. H.; Lai, T. W.; Li, B. H. *J. Catal.* **2009**, *263*, 155.
(9) Chen, C. S.; Lai, T. W.; Chen, C. C. *J. Catal.* **2010**, *273*, 18.
(10) Li, Y.; Fu, Q.; Flytzani-Stephanopoulos, M. *Appl. Catal., B* **2000**, *27*, 179.
(11) Djinović, P.; Batista, J.; Pintar, A. *Appl. Catal., A* **2008**, *347*, 23.
(12) Zerva, C.; Philippopoulos, C. J. *Appl. Catal., B* **2006**, *67*, 105.
(13) Araujo, G. C.; Rangel, M. C. *Catal. Today* **2000**, *62*, 201.
(14) Reddy, B. M.; Khan, A. *Catal. Surv. Asia* **2005**, 155.
(15) Klug, H. P.; Alexander, L. E. *X-ray Diffraction Procedures for Polycrystalline and Amorphous Materials*, 2nd ed.; Wiley: New York, 1974.
(16) Navrotsky, A.; Kleppa, O. J. *J. Inorg. Nucl. Chem.* **1967**, *29*, 2701.
(17) Krawitz, A. D. *Introduction to Diffraction in Materials Science and Engineering*; Wiley-Interscience: New York, 2001.
(18) Boolchand, P.; Pradhan, S.; Wu, Y.; Abdelgadir, M.; Huff, W.; Forell, D.; Coussement, R.; McDaniel, D. *Phys. Rev. B* **1992**, *45*, 921.
(19) Rhodes, C.; Hutchings, G. J.; Ward, A. M. *Catal. Today* **1995**, *23*, 43.
(20) Rhodes, C.; Williams, B. P.; King, F.; Hutchings, G. J. *Catal. Commun.* **2002**, *3*, 381.
(21) Xue, E.; Keeffe, M. O.; Ross, J. R. H. *Catal. Today* **1996**, *30*, 107.
(22) Twigg, M. V. *Catalyst Handbook*, 2nd ed.; Wolfe Publishing: London, 1989; pp 268−288.
(23) Alonso, F. J. P.; Cabrera, I. M.; Granados, M. L.; Kapteijn, F.; Fierro, J. L. G. *J. Catal.* **2006**, *239*, 340.
(24) Lyubutin, I. S.; Lin, C. R.; Korzhetskiy, V.; Dmitrieva, T. V.; Chiang, R. K. *J. Appl. Phys.* **2009**, *106*, 034311.
(25) Rhodes, C.; Williams, B. P.; King, F.; Hutchings, G. J. *Catal. Commun.* **2002**, *3*, 381.
(26) Dumesic, J. A.; Tøpsoe, H. *Adv. Catal.* **1977**, *26*, 121.
(27) Webb, P. A. *MIC Technical Publications*, January 2003; pp 1−12.
(28) Gonzalez, J. C.; Gonzalez, M. G.; Laborde, M. A.; Moreno, N. *Appl. Catal.* **1986**, *20*, 3.
(29) Sastri, M. V. C.; Vishwanath, R. P.; Vishwanath, B. *Int. J. Hydrogen Energy* **1982**, *7*, 951.
(30) Reddy, E. P.; Sun, B.; Panagiotis, P. G. *J. Phys. Chem. B* **2004**, *108*, 17198.
(31) Brown, R.; Cooper, M. E.; Whan, D. A. *Appl. Catal.* **1982**, *3*, 177.
(32) Vandenberghe, R. E.; De Grave, E. In *Mössbauer Spectroscopy Applied to Inorganic Chemistry*; Long, G. J., Grandjean, F., Eds.; Plenum Press: New York, 1989; pp 59−182.
(33) Neel, L. *Ann. Phys.* **1948**, *3*, 137.
(34) Gotic, M.; Jurkin, T.; Music, S. *Mater. Res. Bull.* **2009**, *44*, 2014.
(35) Woude, F. V.; Sawatzky, G. A.; Morrish, A. H. *Phys. Rev.* **1968**, *167*, 533.
(36) Roca, A. G.; Marco, J. F.; Morales, M. P.; Serna, C. J. *J. Phys. Chem. C* **2007**, *111*, 18577.
(37) Wang, J.; Wu, H. Y.; Yang, C. Q.; Lin, Y. L. *Mater. Charact.* **2008**, *59*, 1761.